

## A 2D MATHEMATICAL MODEL ON TRANSONIC AXIAL COMPRESSOR ROTOR FLOW

Árpád VERESS and Imre SÁNTA

Department of Aircraft and Ships  
Budapest University of Technology and Economics  
H-1521 Budapest, Hungary

Received: June 1, 2002

### Abstract

The goal of this project is to develop a new simplified computational method by means of 2D approach to determine the 3D axial compressor rotor performance map. Hence, an inviscid flow solver is reconstructed for transonic flow regime to describe the internal phenomenon. The code is based on two dimensional cell centered shock capturing Euler finite volume scheme using an artificial viscosity and explicit MacCormack's predictor-corrector method for time stepping. For validation, Laval's convergent-divergent nozzle flow and RIZZI, A. W. test case [5] are implemented.

*Keywords:* transonic axial compressor, Euler solver, performance map.

### 1. Introduction

Nowadays, transonic axial compressors are frequently used in engines such as turbojet. In the engineering point of view, the main goal is to reduce weight, complexity and cost, while keeping or improving the given design specifications such as pressure rise or power recovery. Consequently, design engineers are interested in reducing number of compressor stages, assuming that the stage to stage and so the overall pressure ratio is needed to be improved. Generally, in order to develop an advanced compressor, it is necessary to increase not only the aerodynamic loading factor ( $\frac{DH}{U}$ ), but also the rotational speed ( $N$ ), which may mean transonic or supersonic relative inlet Mach number. Such kind of rotor is a transonic or supersonic rotor, for example, in [7].

On the other hand, for a system of conservation laws such as Euler equations model the transonic flow more or less accurately. But it is well known that some dissipation must be introduced in the explicit discretization to control or even prevent the appearance of spurious oscillation. This can be achieved basically in two ways: by introduction of artificial diffusion or by the use of upwind type schemes such as flux vector splitting schemes (e.g. Steger and Warming or van Leer flux vector splitting) or flux difference splitting schemes (Godunov type schemes; e.g. exact, Roe's or Rumsey's approximate Riemann solvers). Following the guideline of Prof. DEGREZ in [1], for the transonic steady flow, for which the shock waves are not too strong, scalar artificial diffusion is probably the best approach. It is computationally inexpensive, simple to program and according to JAMESON [2], 'combined with a

high resolution switching scheme, it captures shock waves in about three interior points'. (In this work this approach has been implemented.) In contrast, for high Mach number flows, associated with strong shock waves and for unsteady flows with moving shock waves, Flux Vector or Flux Difference Upwind Schemes are required. They are more costly but they provide the best possible resolution of shock waves and more important for viscous application and contact discontinuities.

Thirdly, nowadays, the turbomachinery applications of numerical methods for solving 3D Euler/Navier-Stokes equations are widely used all over the world. A huge amount of commercial (e.g. Fluent, CFX – TascFlow) and own codes are available from different sources of scientific literature. The most of compressible Navier-Stokes flow solvers using the high-resolution upwind schemes based on the TVD formulation have been developed by a couple of researchers. DAIGUJI and YAMAMOTO [12], and MATSUO [13] have applied the high-resolution upwind scheme of CHAKRAVARTHY and OSHER [14] with ROE's approximate Riemann solver [15] to transonic cascade flow calculations. FURUKAWA et al. [16] have developed high-resolution upwind finite volume schemes based on a third-order accurate MUSCL approach [17] with the Roe's approximate Riemann solver. In a high-resolution upwind finite difference scheme of YUAN et al. (1993), a fourth-order accurate MUSCL approach with the approximate Riemann solver has been implemented. These codes are able to compute the flow parameters for a given boundary condition. Whereas, in this work the real turbomachinery effect intends to be simulated. How do back pressure and RPM play the role during the operation concerning the inlet mass flow and the inlet flow angle or how can back pressure and RPM fix these parameters. So, the new code is developed, which gives answer for the question and the result of which appears in the performance map. The other goal of this work is to find the most suitable scheme to reduce the huge computational time with using a two dimensional approach.

All the numerical computations were performed at the Center of Information Systems (CIS) of the Budapest University of Technology and Economics on a supercomputer. This serverfarm contains four Compaq 4100 nodes: 16 x EV5.6 (21164A, 600 Mhz, 8 MByte cache) Alpha CPU, 32 GByte memory, 0.62 TByte hard-disc. The nodes communicate by Memory Channel (Full/100 Mb).

## 2. Euler Solver

### 2.1. Governing Equations

The 2 dimensional Euler equation in conservative form appears in the next form:

$$\frac{\partial \mathbf{U}}{\partial t} + \frac{\partial \mathbf{f}}{\partial x} + \frac{\partial \mathbf{g}}{\partial y} = 0 \quad (1)$$

with

$$\begin{aligned}\mathbf{U} &= [\rho, \rho u, \rho v, \rho E]^t, \\ \mathbf{f} &= [\rho u, \rho u^2 + p, \rho uv, (\rho E + p)u]^t, \\ \mathbf{g} &= [\rho v, \rho uv, \rho v^2 + p, (\rho E + p)v]^t,\end{aligned}$$

where  $\rho$  is a density,  $u$  and  $v$  are Cartesian components of velocity,  $p$  is the pressure,  $E$  is the total energy:  $E = e + \frac{u^2 + v^2}{2}$ , and  $e$  is the energy:  $e = C_v T = \frac{1}{\kappa - 1} \frac{p}{\rho}$ . During the computation, normalized variables are used, which are evaluated by the total inlet conditions and typical geometrical length ( $L$ ) and they are next:

$$\begin{aligned}\bar{\rho} &= \frac{\rho}{\rho_0}, & \bar{T} &= \frac{T}{T_0}, & \bar{p} &= \frac{p}{p_0}, & \bar{x} &= \frac{x}{L}, & \bar{y} &= \frac{y}{L}, \\ \bar{a}, \bar{u}, \bar{v} &= \frac{a, u, v}{\sqrt{RT_0}}, & \bar{e}, \bar{E} &= \frac{e, E}{RT_0}, & \bar{t} &= \frac{t}{L} \sqrt{RT_0}\end{aligned}$$

with the formula of sound speed, gas law and energy:

$$\bar{a} = \sqrt{\kappa \bar{T}}, \quad \bar{T} = \frac{\bar{p}}{\bar{\rho}}, \quad e = \frac{\bar{T}}{\kappa - 1}.$$

## 2.2. Cell Centered Finite Volume Spatial Discretization

The spatial discretization starts with setting up a mesh or grid, by which the flow domain is replaced by a finite number of points, in which the numerical values of the variables will be determined. In this work an H-type mesh is used, which symbolizes that the physical domain is divided into the set of grids consisting of pitch-wise lines in  $y$  direction and quasi-streamlines.

A cell centered formulation is used, in which the flow variables are stored at the center of each cell.

Starting from the known values of primitive variables from the previous time step,  $\mathbf{f}$  and  $\mathbf{g}$  are calculated at each cell. After this the line integration is performed for each control volume to calculate the four conserved variables simultaneously. Using the control volume of *Fig. 1*, a semi-discretization of (1) is obtained by

$$\Omega_{i,j} \frac{\partial \mathbf{U}}{\partial t} + \oint_{abcd} \vec{F} \cdot \vec{n} \, dS = 0, \quad (2)$$

where  $\vec{F}$  is a flux vector:  $\vec{F} = \mathbf{f} \vec{e}_x + \mathbf{g} \vec{e}_y$ ,  $dS$  is a surface element,  $\vec{n}$  is the outward normal vector,  $\vec{e}_x$  and  $\vec{e}_y$  are the unit vectors in direction of  $x$  and  $y$  and  $\Omega_{i,j}$  is the volume (area) of  $(i, j)$  element.

By taking a positive direction as indicated in *Fig. 1*:

$$\vec{n} \, dS = dy \vec{e}_x - dx \vec{e}_y. \quad (3)$$

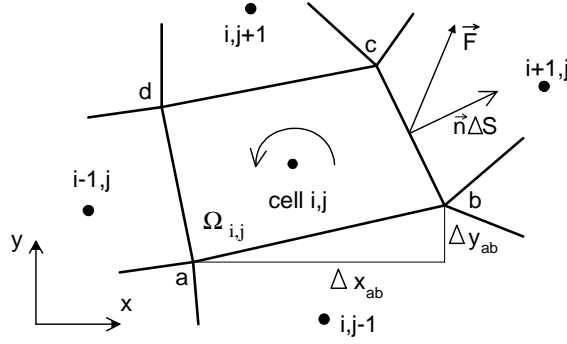


Fig. 1. Cell-centered formulation

Inserting (3) into (2) gives

$$\Omega_{i,j} \frac{\partial \mathbf{U}}{\partial t} + \sum_{abcd} (\mathbf{f} \Delta y - \mathbf{g} \Delta x) = 0 \quad (4)$$

or in detail:

$$\begin{aligned} \Omega_{i,j} \frac{\partial \mathbf{U}}{\partial t} + \mathbf{f}_{ab}(y_b - y_a) - \mathbf{g}_{ab}(x_b - x_a) + \mathbf{f}_{bc}(y_c - y_b) - \mathbf{g}_{bc}(x_c - x_b) \\ + \mathbf{f}_{cd}(y_d - y_c) - \mathbf{g}_{cd}(x_d - x_c) + \mathbf{f}_{da}(y_a - y_d) - \mathbf{g}_{da}(x_a - x_d) = 0. \end{aligned} \quad (5)$$

### 2.3. Artificial Dissipation

All second-order central-discretization schemes, even with a stable time-step, suffer from some instabilities. The problem is that the spurious mode can be defined as an unphysical set of discrete values satisfying the scheme at interior points and vanishing at the nodes where a boundary condition is imposed. By this phenomenon the odd and even mesh points are decoupled and it is caused by the scheme itself. Another problem mean the oscillations, wiggles at steep gradients, such as shock wave and contact discontinuity. The cause is that the discretization is unable to resolve the high frequency content in discontinuities, since the largest waves, which can be resolved on a mesh, have a wavelength of  $2\Delta x$ . In order to make the computation stable and cure the two numerical artefacts described above, some explicitly added higher order dissipation, artificial viscosity may be introduced. In the present work, JAMESON's [2] artificial viscosity is used and Eq. (2) becomes

$$\Omega_{i,j} \frac{\partial \mathbf{U}}{\partial t} + \sum_{abcd} (\mathbf{f} \Delta y - \mathbf{g} \Delta x) - \mathbf{D} = 0, \quad (6)$$

where

$$\mathbf{D} = \mathbf{D}_x + \mathbf{D}_y \quad (7)$$

and

$$\mathbf{D}_x = \mathbf{d}_{i+\frac{1}{2},j} - \mathbf{d}_{i-\frac{1}{2},j}, \quad (8)$$

$$\mathbf{D}_y = \mathbf{d}_{i,j+\frac{1}{2}} - \mathbf{d}_{i,j-\frac{1}{2}}. \quad (9)$$

All the terms on the right side have a similar form, for example, across the cell interface between the nodal values of  $(i, j)$  and  $(i + 1, j)$ :

$$\begin{aligned} \mathbf{d}_{i+\frac{1}{2},j} &= \frac{\Omega_{i,j}}{\Delta t} (\varepsilon_{i+\frac{1}{2},j}^{(2)} (\mathbf{U}_{i+1,j} - \mathbf{U}_{i,j}) \\ &- \varepsilon_{i+\frac{1}{2},j}^{(4)} (\mathbf{U}_{i+2,j} - 3\mathbf{U}_{i+1,j} + 3\mathbf{U}_{i,j} - \mathbf{U}_{i-1,j})). \end{aligned} \quad (10)$$

The coefficients  $\varepsilon^{(2)}$  and  $\varepsilon^{(4)}$  are adapted to the flow with pressure switch define:

$$v_{i,j} = \frac{|p_{i+1,j} - 2p_{i,j} + p_{i-1,j}|}{|p_{i+1,j}| + 2|p_{i,j}| + |p_{i-1,j}|}. \quad (11)$$

Then

$$\varepsilon_{i+\frac{1}{2},j}^{(2)} = \kappa^{(2)} \max(v_{i+1,j}, v_{i,j}), \quad \varepsilon_{i+\frac{1}{2},j}^{(4)} = \max(0, (\kappa^{(4)} - \varepsilon_{i+\frac{1}{2},j}^{(2)})),$$

with the typical values of the constants  $\kappa^{(2)} = \frac{1}{4}$  and  $\kappa^{(4)} = \frac{1}{256}$ .

#### 2.4. Predictor Corrector Technique for Time Stepping

A couple of stable time stepping method, with the appropriate constraints, are possible to apply to solve the ordinary differential equation given by

$$\frac{d\mathbf{U}}{dt} = -\frac{1}{\Omega_{i,j}} \left( \sum_{abcd} (\mathbf{f}\Delta y - \mathbf{g}\Delta x) - \mathbf{D} \right). \quad (12)$$

Although the 4<sup>th</sup> order Runge-Kutta scheme with the frozen dissipative term for the last three stages is one of the most effective methods to solve such a differential equation, in this case, for the sake of simplicity, the MacCormack's predictor-corrector scheme is adopted to FVM to solve it with the biasing of Fig. 2 and the predictor step is

$$\begin{aligned} \bar{\mathbf{U}}_{i,j} &= \mathbf{U}_{i,j}^n - \frac{\Delta t}{\Omega_{i,j}} [\mathbf{f}_{i,j}^n (y_b - y_a) - \mathbf{g}_{i,j}^n (x_b - x_a) \\ &+ \mathbf{f}_{i+1,j}^n (y_c - y_b) - \mathbf{g}_{i+1,j}^n (x_c - x_b) + \mathbf{f}_{i,j+1}^n (y_d - y_c) - \mathbf{g}_{i,j+1}^n (x_d - x_c) \\ &+ \mathbf{f}_{i,j}^n (y_a - y_d) - \mathbf{g}_{i,j}^n (x_a - x_d) - \mathbf{D}^n] = 0 \end{aligned} \quad (13)$$

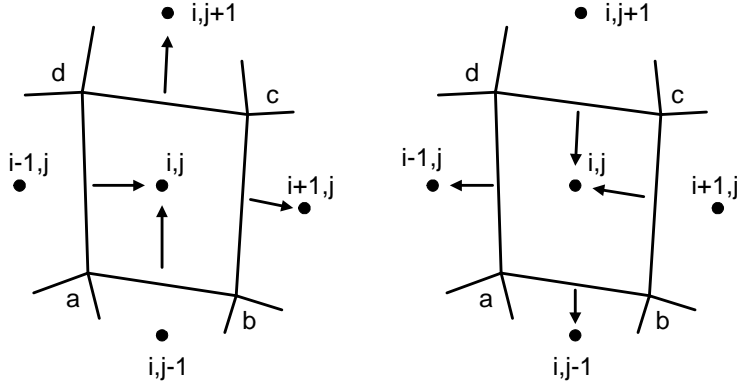


Fig. 2. Predictor and corrector biasing for flux function in MacCormack's method

and corrector step is

$$\begin{aligned} \bar{\bar{\mathbf{U}}}_{i,j} = & \mathbf{U}_{i,j}^n - \frac{\Delta t}{\Omega_{i,j}} [\bar{\mathbf{f}}_{i,j-1}(y_b - y_a) - \bar{\mathbf{g}}_{i,j-1}(x_b - x_a) + \\ & + \bar{\mathbf{f}}_{i,j}(y_c - y_b) - \bar{\mathbf{g}}_{i,j}(x_c - x_b) + \bar{\mathbf{f}}_{i,j}(y_d - y_c) - \bar{\mathbf{g}}_{i,j}(x_d - x_c) \\ & + \bar{\mathbf{f}}_{i-1,j}(y_a - y_d) - \bar{\mathbf{g}}_{i-1,j}(x_a - x_d) - \bar{\mathbf{D}}] = 0. \end{aligned} \quad (14)$$

Finally the next time step is given by

$$\mathbf{U}_{i,j}^{n+1} = \frac{\bar{\mathbf{U}}_{i,j} + \bar{\bar{\mathbf{U}}}_{i,j}}{2}. \quad (15)$$

Concerning the stability, the CFL-restriction for the time step in the MacCormack's scheme is well known and open in literature.

### 2.5. Initial and Boundary Conditions

Data set necessary as an initial and boundary conditions to be imposed with a given system of differential equations, in order to have a well-posed problem.

Due to the hyperbolic nature of the governing equations, the initial conditions do not affect the final solution, but as experienced by the authors, it is not completely arbitrary how to impose it. Normally, a linear variation of pressure is applied between the inlet and outlet planes. Using the isentropic relations and total inlet conditions ( $p_0$ ,  $T_0$ ), only one parameter ( $v$ ) should be imposed to compute all remaining flow variables.

According to the theory of characteristics, if the information propagated by one wave front is impinging a boundary point, coming from the inside of the calculation domain, the value of the corresponding unknown must be calculated from this information and not from a boundary condition. On the other hand, if the information comes from the outside of the calculation domain, the value of the unknown at this boundary point must be imposed by a boundary condition. In 2D, with the projection to the normal of the boundary, the slopes of characteristic curves are  $V_n$ ,  $V_n$ ,  $V_n + a$ ,  $V_n - a$ . These considerations have to be applied in the different boundary problems of a blade-to-blade calculation.

For the inlet boundary, if the velocity is perpendicular to the mesh element and is less than the sound speed, one outgoing and three ingoing characteristics are available. This means that three primitive variables ( $p_0$ ,  $T_0$ ,  $\alpha$ ) must be imposed, while one parameter ( $p$ ) is extrapolated from the interior.

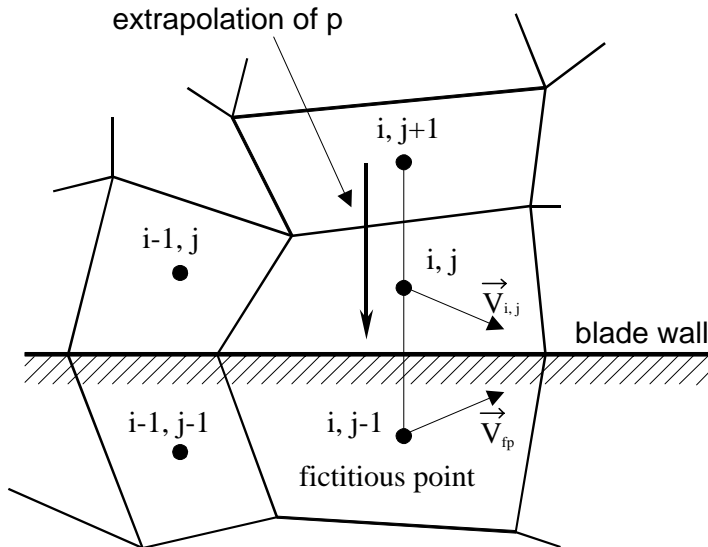


Fig. 3. Mirror-type solid wall model

For the outlet condition, if the velocity is perpendicular to the mesh element and is less than the sound speed, three outgoing and one ingoing characteristics are available. This means that one variable ( $p$ ) must be imposed, while the other three conservative variables ( $\rho$ ,  $\rho u$ ,  $\rho v$ ) are extrapolated from the interior.

As a periodic condition, in the case of blade row computation, before and after the blading the cell rows located at the bounding curves (quasi-streamlines) are coupled. When the discretization uses the nodes of  $(j + 1)$  or  $(j - 1)$  cells at the bounding curve cell rows, the scheme uses the flow data of the opposite cell row, which is staggered with a pitch in positive or in negative  $j$  direction, respectively. So, the infinite number of blade condition is satisfied.

For a solid boundary condition, a mirror type wall model is adopted (Fig. 3). There, only one characteristic enters to the flow domain and only a single physical boundary condition is to be imposed:  $\vec{V}_n = 0$ . As a consequence, all convective flux components through the solid boundary will vanish. This means that only one parameter ( $p$ ) remained to extrapolate from the interior.

### 3. Validation

In order to make sure the correctness of any calculation, a validation is necessary. Generally, the experiments are the best tests to certify our computation, but, because of circumstances, they are not always available. In this case, instead of using supersonic wind tunnel, other validation techniques are applied: Laval's convergent-divergent nozzle flow – to make a comparison between the analytical and numerical calculation for ideal gas and transonic channel flow over a circular arc bump – which test case is widespread for such a transonic flow. Finally, in the last part of the project in Fig. 8 and Fig. 9 a Schlieren photograph is available from literature and numerical results of the solver are found at about the same inlet conditions. The agreement of them, the location and shape of the shock wave are observable quite well.

#### 3.1. 2D Laval's Convergent-Divergent Nozzle Flow

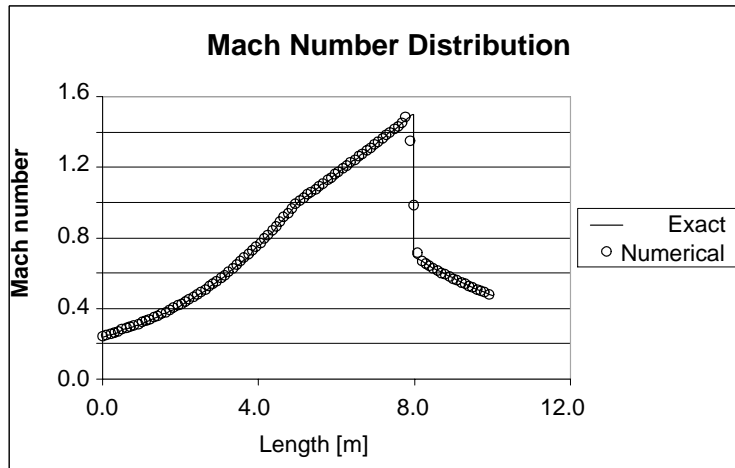


Fig. 4. Mach number distribution along the nozzle

The nozzle shape,  $A = A(x)$ , is divided into two different parts. The first one

is from the reservoir to the throat section described by

$$A(x) = 1 + 1.5 * \left(1 - \frac{x}{5}\right)^2 \quad (16)$$

and the second one from the throat section to the nozzle exit is described by

$$A(x) = 1 + 0.5 * \left(1 - \frac{x}{5}\right)^2, \quad (17)$$

while the length of the channel is 10 meters. For the comparison, the results of the exact and numerical computation (taking the flow parameters along the centerline of the channel meridional section) are shown in *Fig. 4*.

### 3.2. Transonic Channel Flow Over a Circular Arc Bump

This standard test case proposed by RIZZI [5] has been realized. The transonic flow is examined on a relatively coarse grid in the rectangular channel over the circular arc having a maximum thickness of 4.2% in *Fig. 5*. The computational domain is divided into three parts. In the first part,  $x \in [3, 4.35]$ , the grid is stretched towards the bump. In the central part,  $x \in [4.35, 5.65]$ , a constant grid spacing is used. Finally, in the last part of the channel,  $x \in [5.65, 8]$ , the grid is stretched starting from the bump towards the outlet plane. The grid points are distributed as follows:

$$\begin{aligned} x \in [3.00, 4.35] &\longrightarrow i \in [1, 11], \\ x \in [4.35, 5.65] &\longrightarrow i \in (11, 59], \\ x \in [5.65, 8.00] &\longrightarrow i \in (59, 72], \\ y \in [2.96, 5.03] &\longrightarrow j \in (1, 21], \\ x \in [4.50, 5.50] &\longrightarrow i \in (15, 55], \end{aligned}$$

in which the last row refers to the leading and trailing edge of the circular arc. For the stretching function, which is applied in the  $y$  direction also, a simple geometric series type is considered:

$$L = \sum_{i=1}^{N-1} \Delta \xi_i, \quad (18)$$

where  $\Delta \xi_i = \xi_{i+1} - \xi_i$  is constant and predefined,  $L$  is the length to be stretched and  $N$  is the number of points. Let  $R$  be the ratio of two consecutive intervals:

$$R = \frac{\Delta \xi_{i+1}}{\Delta \xi_i}. \quad (19)$$

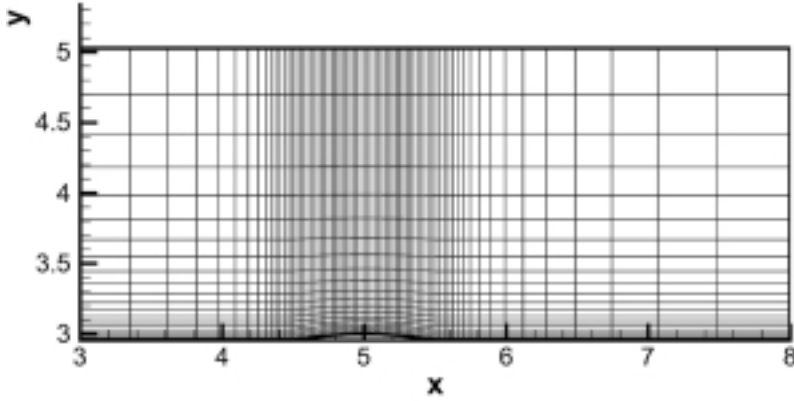


Fig. 5. Channel and a circular arc with H-type grid;  $72 \times 21$  points

The sum of geometric series is given by:

$$L = \Delta\xi_1 \left( \frac{1 - R^N}{1 - R} \right), \quad (20)$$

which, for a given  $N$ ,  $L$ , is a nonlinear function to be solved with a Newton–Raphson method or Fixed Point Iteration [11] for  $R$ , if  $\Delta\xi_1$  is given (and greatest value of  $\Delta\xi_i$ ) and vice versa. The static pressure corresponding to an isentropic flow at Mach = 0.85 is required, provided by the boundary conditions at both inlet and outlet parts of the channel. Under these test conditions the flow expands in the rear part of the bump up to a Mach number of about 1.35, and then ends up into a weak shock wave to allow the recovery of the free stream conditions. In Fig. 6 the Mach iso-lines are shown on grid of  $72 \times 21$  and the relatively sharp shock wave appears in the mentioned region.

#### 4. Transonic Axial Compressor Rotor Performance Map

The main idea of this section is to model the real turbomachinery effects. The rotor speed (RPM) and back pressure determine the mass flow, relative inlet flow angle and total pressure over the blading, if stagnation inlet conditions are fixed. At the inlet, for 2D boundary conditions, the axial velocity ( $u$ ) is calculated in the function of inlet total conditions ( $T_0$ ,  $p_0$ ) and static inlet pressure using isentropic relation

and energy equation:  $\frac{T_0}{T} = \left(\frac{p_0}{p}\right)^{\frac{\kappa-1}{\kappa}}$ ,  $M = \sqrt{\frac{(T_0/T)-1}{\kappa-1} \cdot 2}$ . If the Mach number and static temperature are known, the axial velocity ( $u$ ) (in the case of no prerotation) is easy to compute;  $u = M\sqrt{\kappa RT}$ . While RPM and radial location of the blade element

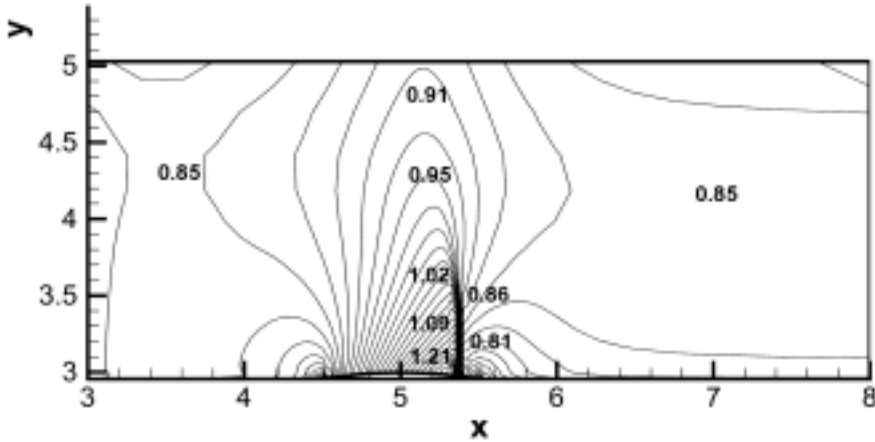


Fig. 6. Mach number distribution over the circular arc in the transonic channel

are given, the peripheral velocity ( $v$ ) and finally the asked boundary condition: the relative flow angle ( $\alpha$ ) can be determined.

In this work NACA RM E52C27 [7] transonic rotor blade section, which is the nearest to the tip, is used for construction 2D cascade to make a computational investigation and set up the performance map (Fig. 7). Of course this approach is only for demonstration (because of absence of measurements) and it tries to show how the transonic flow behaves in turbomachinery.

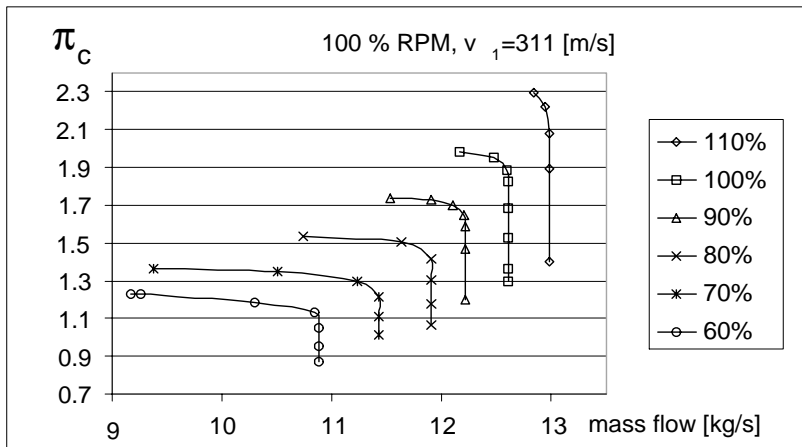


Fig. 7. Compressor rotor map over one pitch (per unit blade height)

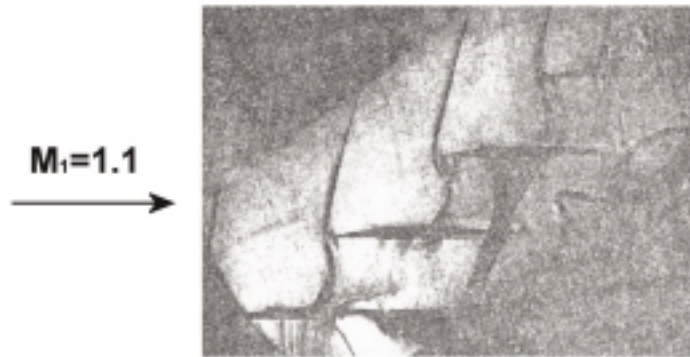


Fig. 8. Schlieren photograph shows the shock wave pattern [9]

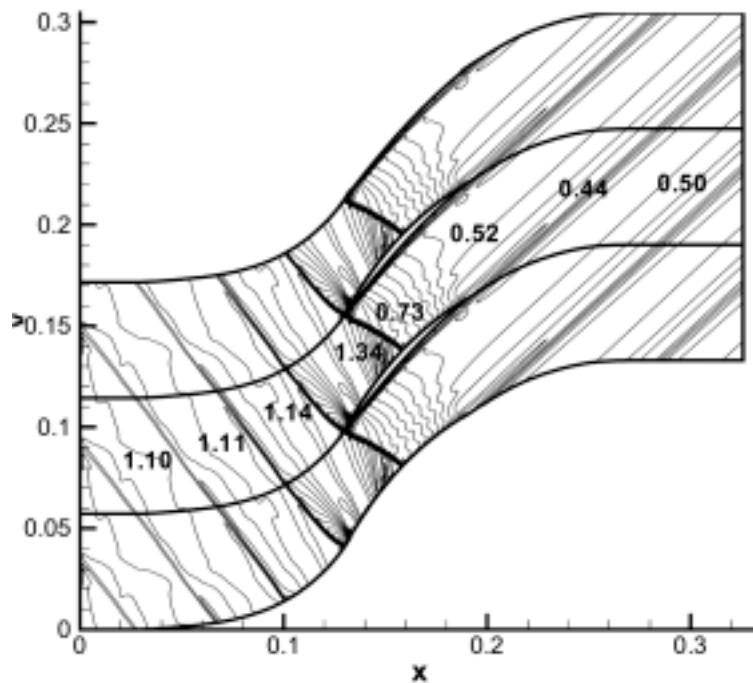


Fig. 9. Mach number distribution by computation

For the further investigations a question is remaining to answer. How to model the 3D rotor in 2D. First, the blading is divided into the annular segments by an axis-symmetric surface from hub to tip, parallel to the axis. Although the machine

in meridional plane is converging, an average and constant meridional passages are used between leading and trailing edge. The blade profile, which is located at the middle part of each segment with the belonging flow parameter provided by the solver are assumed to be constant for the regarding segment. On the other hand, an analytical correction is adopted in the solver, which takes the difference between the inlet and outlet cross section per segment into consideration with the next simple iteration:

1. Conservation balance of mass for  $u'_2$ , while  $\rho'_2$  is the returning variable of iteration:

$$\dot{m} = A_1 u_2 \rho_2 = A_2 u'_2 \rho'_2. \quad (21)$$

2. Conservation of energy for  $T'_2$  with  $V'^2 = u'^2 + v'^2$ :

$$C_p T_2 + \frac{V_2^2}{2} = C_p T'_2 + \frac{V'^2_2}{2}. \quad (22)$$

3. Poisson equation for  $p'_2$ :

$$\frac{T'_2}{T_2} = \left( \frac{p'_2}{p_2} \right)^{\frac{\kappa-1}{\kappa}}. \quad (23)$$

4. And finally the gas law for the variable of iteration ( $\rho'_2$ ):

$$\frac{p'_2}{\rho'_2} = R T'_2. \quad (24)$$

The iteration loop is continued until the first equation is satisfied. The marked static pressure is going to be the outlet boundary condition for the scheme and it corresponds to the narrower flow path, which belongs to outlet plane  $A_2$  per segment. During the computation all flow parameters are computed by mass flow averaging in the performance map (*Fig. 7*).

## 5. Conclusion

Jamenson's artificial viscosity technique is re-developed and used to solve the Euler's equations in 2D, tested for transonic flow and applied to evaluate a transonic axial compressor rotor performance map. Hence, the inlet boundary condition is slightly modified in such a way that mass flow and inlet flow angle feel the effect of back pressure, which is typical of the compressors. This procedure makes a connection between the absolute and relative flow parameters. Although, in 2D approach, the centrifugal and coriolis force are skipped, this approach is used to save computational time and describe the flow field in 3D. Hence, a simple analytical approach is used with a simple technique, which makes a relation between 2D and 3D, to establish a 3D compressor rotor map.

## List of Symbols

### Variables

$a$	Sound speed [m/s]
$\mathbf{D}$	Dissipative flux vector
$C_v$	Specific heat [J/(kgK)]
$dS$	Surface element [m]
$e$	Static energy [J/kg]
$\vec{e}$	Unit vector
$E$	Total energy [J/kg]
$\mathbf{f}$	Convective flux vector ( $x$ component)
$\mathbf{g}$	Convective flux vector ( $y$ component)
$\dot{m}$	Mass flow [kg/s]
$M$	Mach number
$\vec{n}$	Outward pointing normal
$R$	Perfect gas constant [J/(kgK)]
$t$	Time [s]
$T$	Temperature [K]
$u$	$x$ component of velocity vector [m/s]
$\mathbf{U}$	Vector of conservative variables
$x, y$	Space variables
$v$	$y$ comp. of velocity vector [m/s]
$\vec{V}$	Velocity vector of comp. ( $u, v$ )
$\alpha$	Flow angle
$\kappa$	Constant specific heat
$\rho$	Density [kg/m <sup>3</sup> ]
$\Omega$	Cell volume (area) [m <sup>2</sup> ]

### Indices

1	Rotor inlet conditions
2	Rotor outlet conditions
'	Refers to corrected values
$o$	Total or stagnation condition
–	Refers to normalized form and results of predictor step
$abcd$	Refers to quadrilateral cell
$i, j$	Cell or spatial indices
$n$	Time level
$n$	Normal to boundary
$x, y$	Refer to space variables
$v$	Refers to constant volume

## References

- [1] DEGREZ, G., Implicit Time Dependent Methods for Inviscid and Viscous Compressible Flows, with a Discussion of the Concept of Numerical Dissipation. *Annual Lecture Series at VKI: Introduction to Computational Fluid Dynamics*, 2000.
- [2] SCHMIDT, W. – JAMESON, A., Recent Developments in Finite-Volume Time-Dependent Techniques for Two and Three Dimensional Transonic Flows. *Lecture Series at VKI: Computational Fluid Dynamics*, 1982.
- [3] SÁNTA, I., Transzszónikus Kompresszor Fokozatok. *Oktatási segédanyag, BME, Repülőgépek és Hajók Tanszék, Budapest*, 2002.
- [4] DICK, E., Introduction to Finite Volume Techniques in Computational Fluid Dynamics. *Annual Lecture Series at VKI: Introduction to Computational Fluid Dynamics*, 2000.
- [5] RIZZI, A. W., Numerical Methods for the Computations of Transonic Flows with Shock Waves. *Notes on Numerical Fluid Mechanics*, Vieweg, Braunschweig 3, 1981.
- [6] VERESS, Á., Inverse Design on Return Flow Channel for Multistage Radial Compressor. *VKI Diploma Course Project Report 2001-27*, 2001.
- [7] LEWIS, G. W. Jr., Experimental Investigation of Axial-Flow Compressor Inlet Stage Operating at Transonic Relative Inlet Mach Numbers, II-Blade Coordinate Data. *NACA Research Memorandum (RM E52C27), National Advisory Committee for Aeronautics Washington*, 1952.
- [8] VERESS, Á., Bevezetés az áramlástan numerikus módszereibe. *Oktatási segédanyag, BME, Repülőgépek és Hajók Tanszék, Budapest*, 2002.
- [9] STARKE, H., Untersuchung der Strömung in ebenen Überschallverzögerungsgittern. *DLR-Forschungsbericht 71-99*, 1971.
- [10] VERESS, Á., Simplified Method on Mathematical Model of Transonic Axial Compressors. *22nd ICAS Proceedings: ICA0775P*, Harrogate, UK, 2000.
- [11] HÜTTE, A mérnöki tudományok kézikönyve, A108 pp. Springer-Verlag, 1993.
- [12] DAIGUJI, H. – YAMAMOTO, S., Numerical Methods for Transonic Cascade Flow Problems. *A Collection of Technical Papers: International Symposium on Computational Fluid Dynamics-Nagoya*, (1989), pp. 548–553.
- [13] MATSUO, Y., Computations of Three Dimensional Viscous Flows in Turbomachinery Cascades. *AIAA Paper No. 91-2237*, (1991).
- [14] CHAKRAVARTHY, S. R. – OSHER, S., A New Class of High Accuracy TVD Scheme for Hyperbolic Conservation Laws. *AIAA Paper No. 85-0363*, 1985.
- [15] ROE, P. L., Approximate Riemann Solvers, Parameter Vectors, and Difference Schemes. *Journal of Computational Physics*, **43** (1981), pp. 357–372.
- [16] FURUKAWA, M. – YAMASAKI, M. – INOUE, M., A Zonal Approach for Navier-Stokes Computations of Compressible Cascade Flow Fields Using a TVD Finite Volume Method. *ASME Journal of Turbomachinery*, **113** No. 4 (1991), pp. 573–582.
- [17] ANDERSON, W. K. – THOMAS, J. L. – VAN LEER, B., Comparison of Finite Volume Flux Vector Splitting for the Euler Equations. *AIAA Journal*, **24** No. 9 (1986), pp. 1453–1460.